LETTER

doi:10.1038/nature16495

Powering Earth's dynamo with magnesium precipitation from the core

Joseph G. O'Rourke[1] & David J. Stevenson[1]

Earth's global magnetic field arises from vigorous convection within the liquid outer core. Palaeomagnetic evidence reveals that the geodynamo has operated for at least 3.4 billion years[1], which places constraints on Earth's formation and evolution. Available power sources in standard models include compositional convection (driven by the solidifying inner core's expulsion of light elements), thermal convection (from slow cooling), and perhaps heat from the decay of radioactive isotopes. However, recent first-principles calculations[2,3] and diamond-anvil cell experiments[4,5] indicate that the thermal conductivity of iron is two or three times larger than typically assumed in these models. This presents a problem: a large increase in the conductive heat flux along the adiabat (due to the higher conductivity of iron) implies that the inner core is young (less than one billion years old[4]), but thermal convection and radiogenic heating alone may not have been able to sustain the geodynamo during earlier epochs. Here we show that the precipitation of magnesium-bearing minerals from the core could have served as an alternative power source. Equilibration at high temperatures in the aftermath of giant impacts allows a small amount of magnesium (one or two weight per cent) to partition into the core while still producing the observed abundances of siderophile elements in the mantle and avoiding an excess of silicon and oxygen in the core. The transport of magnesium as oxide or silicate from the cooling core to underneath the mantle is an order of magnitude more efficient per unit mass as a source of buoyancy than inner-core growth. We therefore conclude that Earth's dynamo would survive throughout geologic time (from at least 3.4 billion years ago to the present) even if core radiogenic heating were minimal and core cooling were slow.

Earth differentiated into a silicate mantle and an iron-rich core during its formation in the approximately 100 million years following the initial collapse of the solar nebula. Scores of collisions between planetary embryos ranging from Moon- to Mars-sized accompanied by an influx of smaller planetesimals characterized the last stage of accretion[6,7]. In one view of core formation, impacting embryos disaggregate in a deep magma ocean that overlies a mostly solid region[8–12]. Metal sinks into a pond at the base of the magma ocean and equilibrates at the ambient pressure and temperature near the peridotite liquidus. As a consequence, the mantle becomes depleted in siderophile elements. Metallic diapirs quickly sink to the core–mantle boundary (CMB) without further equilibration, although percolation through the lower mantle has also been suggested[13]. One issue with this view is that the concentration of light elements in core material should increase over time as pressure and temperature increase. Without vigorous mixing, a stable compositional stratification would develop below the CMB[14], which could prevent the initialization of a convective dynamo. The Moon-forming giant impact and possibly earlier, less energetic ones may recover the homogeneity of the core. Giant impacts are also important because they can heat parts of Earth to around 10,000 K, possibly even causing complete melting[15–17]. Portions of the cores of large impactors should emulsify down to short (centimetres) length scales in the superheated mantle[18], permitting some metal–silicate equilibration at temperatures far above the peridotite liquidus.

The density of the core today, inferred from seismology, is about 10% less than the expected value for a pure iron/nickel (Fe/Ni) alloy at the high temperatures and pressures of Earth's deep interior[19]. Identifying the light element(s) responsible for this deficit has remained a central problem for decades. Despite being the fourth most abundant element in Earth by mass, magnesium (Mg) has been correctly rejected as a major contributor to the density deficit of the core in favour of elements like S, Si, O, C, and H, since Mg (as an oxide or silicate) and metallic Fe are almost immiscible under ambient conditions[19].

However, the complete absence of Mg from the core is a thermodynamic impossibility because of entropic effects. New first-principles calculations indicate that the saturation limit of MgO in Fe is below 0.1 mol% at 3,000 K and 50 GPa, but reaches 1 mol% at 4,200 K and increases rapidly thereafter[20]. Partitioning studies in diamond-anvil cells likewise indicate that Mg is not present above the detection limit after equilibration below 3,000 K. But Mg abundances approaching 1 mol% are observed in experiments reaching 3,000 K to 5,000 K (refs 21, 22). Spurious signals from the surrounding silicate are a complicating factor in these experiments, given the small sample sizes[22]. Still, all available data are consistent with the solubility of Mg in the Fe-rich metal exhibiting an exponential (Arrhenius) dependence on temperature. The low solubility also necessarily implies a strong dependence of that solubility on temperature.

Here we demonstrate that the composition of the mantle is consistent with core–mantle differentiation partially occurring at temperatures that permit substantial Mg partitioning. We consider two simple models of Earth's accretion, assuming that Earth is comprised of 12 major (Fe, Si, and O), lithophile (Mg, Al, and Ca), and siderophile (Ni, Co, Cr, V, Nb, and Ta) elements. First, we test a conventional, single-stage model with equilibration temperatures near the peridotite liquidus at mid-mantle depths. Second, we develop a two-stage model with some material equilibrating at temperatures above 5,000 K. To calculate the composition of Earth's core and mantle, we adopt parameterizations of partition coefficients (the metal-to-silicate ratio of elemental concentrations) as functions of pressure, temperature, and bulk composition from the most recent and comprehensive data sets[12,22]. We compare the predictions of our models to the estimated composition of the primitive mantle and the core mass fraction[23].

A Markov chain Monte Carlo analysis quantifies the distribution of model parameters that match the available data. This technique explores the effects of varying all variables within their plausible uncertainties, with tens of orders of magnitude more computational efficiency than a simple grid search of the high-dimensional parameter space. The median chi-squared values are 8.3 and 8.6 for the single- and two-stage models, respectively, indicating that both models can provide good fits to the data. Figure 1 shows that our two-stage model reproduces the observed elemental abundances in the primitive mantle. That is, the peaks of the probability density functions are all within 0.83σ of the estimated mean values. The median result of this model is

[1]Division of Geological and Planetary Sciences, California Institute of Technology, Pasadena, California 91125, USA.

© 2016 Macmillan Publishers Limited. All rights reserved

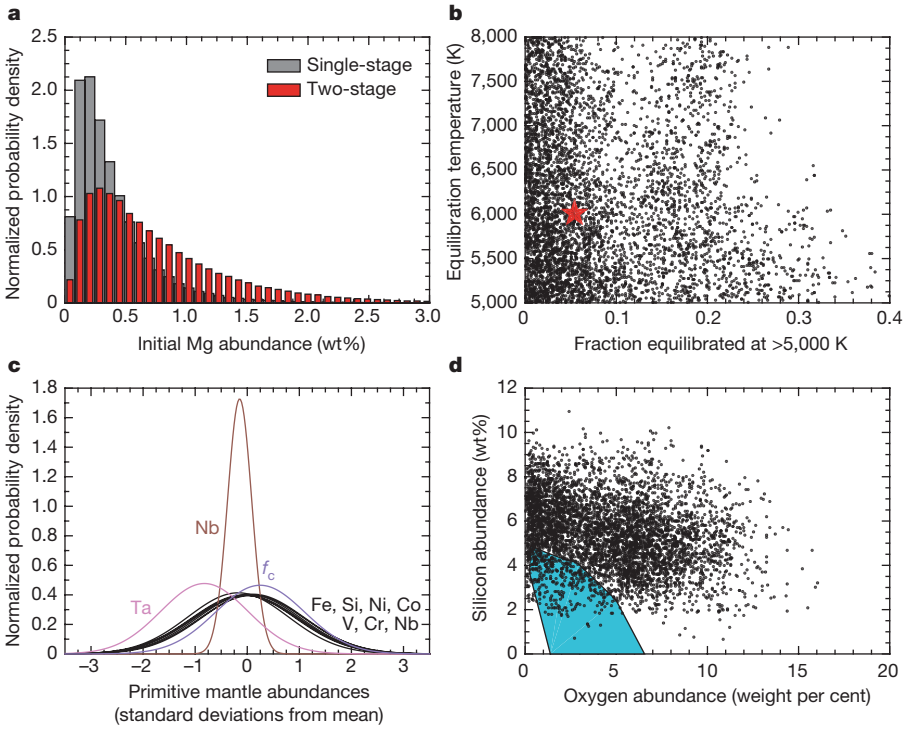

Figure 1 | Composition of Earth's core and mantle immediately after accretion from models of silicate–metal equilibrium. a, Initial abundance of Mg in the core from both models. **b**–**d**, From the two-stage model: fraction of material (red star is the mean result) equilibrated in the aftermath of giant impacts (**b**), posterior probability densities for elemental abundances in the primitive mantle[23] and the core mass fraction, f_c (**c**), and the initial abundances of Si and O in the core compared to those permitted (blue region) by present-day seismological observations[24] (**d**). Black dots are random draws from the posterior distributions.

that ~5 wt% of Earth equilibrates at ~6,000 K, although the equilibration of up to ~20 wt% at 8,000 K is permissible if other parameters are suitably adjusted. Mirroring previous studies, our single-stage model suggests a best-fit equilibration pressure of 57 ± 9 GPa, corresponding to 3,500 ± 250 K. Without partial equilibration at higher temperatures, less than 0.5 wt% Mg is expected to enter the core. The two-stage model, however, permits initial Mg abundances ranging from ~0.5 wt% to 2 wt%.

Other light elements also enter the core as temperatures of equilibration increase. Figure 1 illustrates that siderophile elements alone do not tightly constrain the initial abundances of Si and O in the core, especially since calculating partitioning behaviour above 5,000 K necessitates extrapolating the available experimental data[22]. Some two-stage simulations yield compositions within the 1σ range of estimated values for the present-day core based on seismology and mineral physics[24]. But our models seem to 'prefer' slightly higher initial abundances of light elements. Precipitation caused by rapidly decreasing Mg solubility in the cooling core can lower the abundances of Si and, especially, O to their modern values.

Figure 2 shows representative calculations of the precipitation of Mg-bearing silicates and oxides from Earth's core. Here we assume that the core initially contained 3 wt% Si and 6 wt% O. We find that the amount of mass precipitated as a function of temperature is a sensitive function of the solubility of O, along with the expected dependence on the initial Mg abundance. Using the mean exchange coefficient for Mg, at least 1 wt% Mg is required for precipitation to begin above 4,000 K. Alternatively, the constants used to calculate the exchange coefficient for O could be decreased by more than 0.25σ from their estimated mean values. Extended Data Fig. 1 illustrates one example of the evolving composition of the precipitate. The solubility of Mg is below that of Si and O, so it comprises almost half the precipitate by number despite having the lowest abundance. The precipitate becomes more Si-rich as Mg is depleted, whereas the Fe content remains roughly constant. Overall, ~0.5% of the initial mass precipitates per 100 K of cooling once precipitation begins.

Transporting precipitated material to the CMB from a mostly well-mixed outer core releases more gravitational energy per unit mass than inner-core growth. Large-scale vertical motions are necessary to maintain the dynamo, meaning that either thermal or compositional effects must provide enough buoyancy to keep the temperature profile in the liquid outer core close to the adiabat in the region of dynamo generation[25,26]. Crucially, the density difference between the precipitate and the outer core is approximately ten times the contrast between the inner and outer core attributable to composition (roughly half of the ~5% total). This means that precipitating a layer of Mg-bearing material with a thickness of only ~10 km above the CMB is energetically equivalent to crystallizing the entire inner core. We incorporate Mg precipitation into comprehensive models of the energetics of the core to explore its importance further.

Figure 3 presents several calculations for the thermochemical evolution of the core. We iterate the equations of global energy and entropy balance backwards in time from present-day conditions[26]. Given a fixed amount of entropy production, we calculate the CMB heat flow and cooling rate necessary to sustain the dynamo. We use the recently

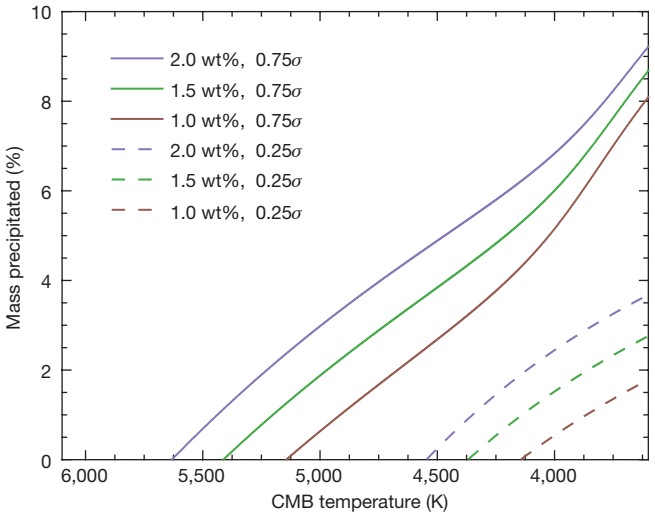

Figure 2 | Estimates of mass precipitated from the cooling core. The colours denote initial Mg abundances, while solid and dashed lines represent calculations with the constants a_O, b_O, and c_O used to calculate O solubility (K_O) decreased by different fractions of a standard deviation.

© 2016 Macmillan Publishers Limited. All rights reserved

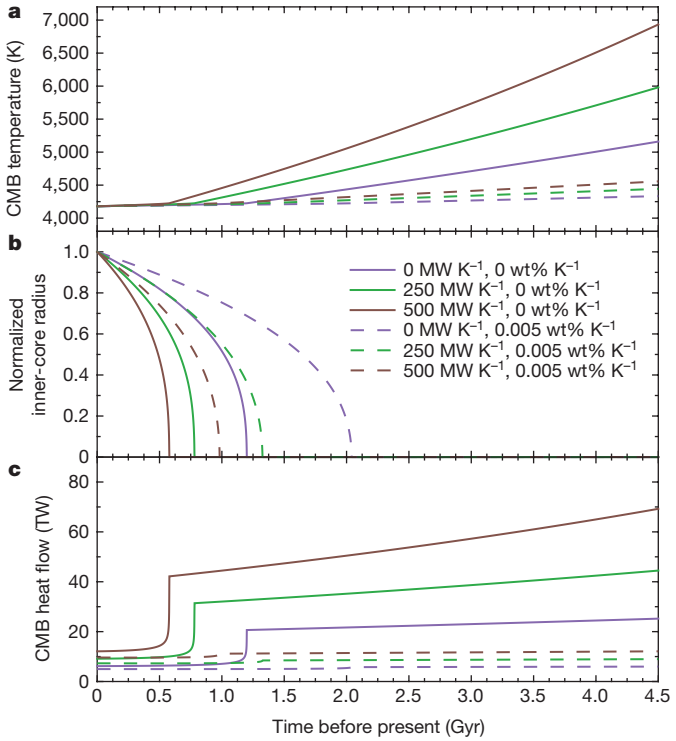

Figure 3 | Thermochemical evolution of the core for various rates of precipitation and entropy production associated with ohmic dissipation. Assuming that the core always produces a constant amount of entropy required to sustain the dynamo, we calculate the implied CMB temperature (**a**), inner-core radius relative to the present (**b**), and CMB heat flow (**c**). Gyr, billion years.

revised value of core thermal conductivity, despite a new study[27] that militates against the emerging theoretical and experimental consensus[2–5]. If there is no Mg precipitation, an entropy production rate of 500 MW K^{-1} (corresponding to ~2.5 TW of ohmic dissipation) implies initial CMB temperatures of ~7,000 K and a core-to-mantle heat flow of 40 TW to 70 TW before inner-core nucleation at ~0.6 billion years ago. Incorporating the plausible precipitation rate lowers the necessary amount of secular cooling to only ~300 K over 4.5 billion years. A core heat flow close to the present-day value (<20 TW) is thus sufficient to power a dynamo for Earth's entire history.

Precipitation of Mg from the core has profound implications for the evolution of Earth's deep interior. Most importantly, it eliminates the need to invoke a geochemically dubious magnitude of radiogenic heating[28] or enhanced heat flux across the CMB into a basal magma ocean[29]. High thermal conductivity and slow core cooling are consistent with inner-core nucleation in the Mesoproterozoic[30]. Models that include only the inner core as a source of compositional buoyancy predict that stable layers hundreds of kilometres thick should develop near the CMB[3], which may be disrupted by precipitation. However, precipitation may actually occur at depth if the solubility of Mg is strongly pressure dependent. The real situation is even more complicated if the CMB is undersaturated in Si and O, meaning that material from the mantle tends to dissolve in the core. Elemental transport in both directions is potentially permissible because the Mg-rich precipitate differs in composition from the CMB. The effect of giant impacts on core formation should motivate additional experiments on metal–silicate partitioning at temperatures above 5,000 K. Non-standard evolutionary scenarios featuring precipitation are perhaps applicable to the cores of other terrestrial planets.

Online Content Methods, along with any additional Extended Data display items and Source Data, are available in the online version of the paper; references unique to these sections appear only in the online paper.

Received 9 January; accepted 26 November 2015.

1. Tarduno, J. A. *et al.* Geodynamo, solar wind, and magnetopause 3.4 to 3.45 billion years ago. *Science* **327,** 1238–1240 (2010).
2. de Koker, N., Steinle-Neumann, G. & Vlcek, V. Electrical resistivity and thermal conductivity of liquid Fe alloys at high *P* and *T*, and heat flux in Earth's core. *Proc. Natl Acad. Sci. USA* **109,** 4070–4073 (2012).
3. Pozzo, M., Davies, C., Gubbins, D. & Alfe, D. Thermal and electrical conductivity of iron at Earth's core conditions. *Nature* **485,** 355–358 (2012).
4. Gomi, H. *et al.* The high conductivity of iron and the thermal evolution of the Earth's core. *Phys. Earth Planet. Inter.* **224,** 88–103 (2013).
5. Seagle, C. T., Cottrell, E., Fei, Y., Hummer, D. R. & Prakapenka, V. B. Electrical and thermal transport properties of iron and iron-silicon alloy at high pressure. *Geophys. Res. Lett.* **40,** 5377–5381 (2013).
6. Chambers, J. E. Planetary accretion in the inner Solar System. *Earth Planet. Sci. Lett.* **223,** 241–252 (2004).
7. Ogihara, M., Ida, S. & Morbidelli, A. Accretion of terrestrial planets from oligarchs in a turbulent disk. *Icarus* **188,** 522–534 (2007).
8. Wade, J. & Wood, B. J. Core formation and the oxidation state of the Earth. *Earth Planet. Sci. Lett.* **236,** 78–95 (2005).
9. Wood, B. J., Walter, M. J. & Wade, J. Accretion of the Earth and segregation of its core. *Nature* **441,** 825–833 (2006).
10. Rubie, D. C. *et al.* Heterogeneous accretion, composition and core-mantle differentiation of the Earth. *Earth Planet. Sci. Lett.* **301,** 31–42 (2011).
11. Siebert, J., Badro, J., Antonangeli, D. & Ryerson, F. J. Terrestrial accretion under oxidizing conditions. *Science* **339,** 1194–1197 (2013).
12. Rubie, D. C. *et al.* Accretion and differentiation of the terrestrial planets with implications for the compositions of early-formed Solar System bodies and accretion of water. *Icarus* **248,** 89–108 (2015).
13. Shi, C. Y. *et al.* Formation of an interconnected network of iron melt at Earth's lower mantle conditions. *Nature Geosci.* **6,** 971–975 (2013).
14. Helffrich, G. Outer core compositional layering and constraints on core liquid transport properties. *Earth Planet. Sci. Lett.* **391,** 256–262 (2014).
15. Canup, R. M. Accretion of the Earth. *Phil. Trans. R. Soc. A* **366,** 4061–4075 (2008).
16. Canup, R. M. Forming a Moon with an Earth-like composition via a giant impact. *Science* **338,** 1052–1055 (2012).
17. Cuk, M. & Stewart, S. T. Making the Moon from a fast-spinning Earth: a giant impact followed by resonant despinning. *Science* **338,** 1047–1052 (2012).
18. Dahl, T. & Stevenson, D. J. Turbulent mixing of metal and silicate during planet accretion—and interpretation of the Hf-W chronometer. *Earth Planet. Sci. Lett.* **295,** 177–186 (2010).
19. Poirier, J. Light elements in the Earth's outer core: a critical review. *Phys. Earth Planet. Inter.* **85,** 319–337 (1994).
20. Wahl, S. M. & Militzer, B. High-temperature miscibility of iron and rock in terrestrial planet formation. *Earth Planet. Sci. Lett.* **410,** 25–33 (2015).
21. Takafuji, N., Hirose, K., Mitome, M. & Bando, Y. Solubilities of O and Si in liquid iron in equilibrium with $(Mg,Fe)SiO_3$ perovskite and the light elements in the core. *Geophys. Res. Lett.* **32,** L06313 (2005).
22. Fischer, R. A. *et al.* High pressure metal-silicate partitioning of Ni, Co, V, Cr, Si, and O. *Geochim. Cosmochim. Acta* **167,** 177–194 (2015).
23. Palme, H. & O'Neill, H. in *Treatise on Geochemistry* 2nd edn (eds Holland, H. & Turekian, K.) 1–39 (Elsevier, 2013).
24. Badro, J., Cote, A. S. & Brodholt, J. P. A seismologically consistent compositional model of Earth's core. *Proc. Natl Acad. Sci. USA* **111,** 7542–7545 (2014).
25. Stevenson, D. J. Planetary magnetic fields. *Earth Planet. Sci. Lett.* **208,** 1–11 (2003).
26. Nimmo, F. in *Treatise on Geophysics* 2nd edn (ed. Schubert, G.) 31–65 (Elsevier, 2015).
27. Zhang, P., Cohen, R. E. & Haule, K. Effects of electron correlations on transport properties of iron at Earth's core conditions. *Nature* **517,** 605–607 (2015).
28. Corgne, A., Shantanu, K., Fei, Y. & McDonough, W. F. How much potassium is in the Earth's core? New insights from partitioning experiments. *Earth Planet. Sci. Lett.* **256,** 567–576 (2007).
29. Labrosse, S., Hernlund, J. W. & Coltice, N. A crystallizing dense magma ocean at the base of the Earth's mantle. *Nature* **450,** 866–869 (2007).
30. Biggin, A. J. *et al.* Palaeomagnetic field intensity variations suggest Mesoproterozoic inner-core nucleation. *Nature* **526,** 245–248 (2015).

Acknowledgements This material is based upon work supported by the National Science Foundation Graduate Research Fellowship under grant number DGE-1144469 (J.G.O'R.).

Author Contributions J.G.O'R. performed the calculations and wrote the manuscript. D.J.S. designed the project, discussed the results, and commented on the manuscript.

Author Information Reprints and permissions information is available at www.nature.com/reprints. The authors declare no competing financial interests. Readers are welcome to comment on the online version of the paper. Correspondence and requests for materials should be addressed to J.G.O'R. (jorourke@caltech.edu).

© 2016 Macmillan Publishers Limited. All rights reserved

METHODS

Element partitioning. For an element M besides oxygen with valence n, the partition coefficient is defined as $D_M = X^{met}{}_M / X^{sil}{}_{MO_{n/2}}$, where $X^{met}{}_M$ is the mole fraction of the element M in metal and $X^{sil}{}_{MO_{n/2}}$ is the mole fraction of the corresponding oxide $MO_{n/2}$ in the silicate[22]. The associated exchange coefficient is $K_M = D_M / D_{Fe}{}^{n/2}$. For oxygen, $K_O = X^{met}{}_{Fe} X^{met}{}_O / X^{sil}{}_{FeO}$. Using experimental data, the exchange coefficients K_M may be parameterized as follows[22]:

$$\log_{10} K_M = a_M + \frac{b_M}{T} + \frac{c_M P}{T} + \frac{\varepsilon_M^M \ln(1-X_M)}{2.303} + \frac{1}{2.303}\sum_{\substack{k=1\\k\neq i}}^{N} \varepsilon_k^i X_k \left(1 + \frac{\ln(1-X_k)}{X_k} - \frac{1}{1-X_i}\right) - \frac{1}{2.303}\sum_{\substack{k=1\\k\neq i}}^{N} \varepsilon_k^i X_k^2 X_i \left(\frac{1}{1-X_i} + \frac{1}{1-X_k} + \frac{X_i}{2(1-X_i)^2} - 1\right)$$

where P is pressure, and a_M, b_M and c_M are constants. Each ε_j^i is the interaction parameter of elements i and j in the liquid at temperature T, which is a function of the reference interaction parameter e_j^i determined at a reference temperature of 1,873 K. These compositional parameters are necessary to fit partitioning data for V and Cr, but are typically set to zero for other siderophile elements[22].

We estimate a_{Mg} and b_{Mg} using experimental results from ref. 21 and assuming that 0.05 wt% of Mg (below the detection limit) was present in quenched liquid iron at 2,500 K. Our derived values are in agreement with theoretical predictions[20] and preliminary results from diamond-anvil cell experiments at higher temperatures[31]. We adopt formal errors (100% and 9%, respectively) for these parameters a_{Mg} and b_{Mg}, which are comparable in magnitude to those for other elements[22]. We assume here that $c_{Mg} = 0$ and that interaction effects are negligible, although future experiments may reveal that these factors actually are important.

Equations for the exchange coefficients and mass balance allow us to solve for the composition of the metal and silicate phases for any initial bulk composition, given the temperature and pressure of equilibration. Methods for solving these equations are detailed by Rubie *et al.*[10,12] and others[11,22]. Since the valences of elements in the silicates are specified, oxygen fugacity is not a free parameter. Extended Data Table 1 lists experimentally determined values for all constants in our models, along with their formal errors.

Core formation. We consider two simple scenarios for Earth's accretion and differentiation. Both models have 37 parameters with quantified uncertainties corresponding to the oxygen-free composition of bulk Earth[32] and the constants used to calculate partitioning behaviour[12,22]. Our single-stage model has two additional parameters: P_1, the pressure at equilibration, and $[Fe/O]_1$, the ratio of the molar abundances of iron and oxygen in bulk Earth. In this case, we assume that equilibration occurs at the base of a magma ocean with temperature on the peridotite liquidus. In our two-stage model, we permit a fraction of Earth to equilibrate at T_2 between 5,000 K and 8,000 K, which is hotter than the peridotite liquidus at the CMB. This material may equilibrate at a different pressure, P_2, and can also have a different bulk oxygen content, $[Fe/O]_2$. We restrict P_1 and P_2 between 0 GPa and 135 GPa with equal prior probability throughout this range. Likewise, we allow $0.25 < [Fe/O]_1 < 0.65$ and $0.25 < [Fe/O]_2 < 0.6$, representing a range of oxidizing and reducing conditions. For reference, the best-fit $[Fe/O]_1 = 0.52 \pm 0.02$ in the single-stage model. We aim to reproduce ten data points: the estimated abundances of Fe, Si, Ni, Co, V, Cr, Nb and Ta in the primitive mantle, along with the ratio Nb/Ta (14.0 ± 0.3) and the core mass fraction, f_c (0.32 ± 0.01).

Given the high dimensionality of our models, a comprehensive grid search is computationally prohibitive. The Markov chain Monte Carlo technique, however, samples only each point in the parameter space that has a frequency equal to the posterior probability at that point. We use the standard Metropolis–Hastings sampling[33]. Briefly, we begin with an initial guess for the model parameters, N_x. To decide whether to add another set of model parameters, N_{x+1}, to the chain, we compute the likelihood and prior probability. The posterior probability, $p(N_x)$, is proportional to the multiple of the likelihood and the prior. The likelihood is proportional to the conventional chi-squared value computed from the difference between the model output and the data. The prior is determined from experimental constraints. For example, a model that sets all constants used to calculate partitioning behaviour equal to their mean estimated values has a higher prior than a model where a few constants are increased or decreased by a fraction of a standard deviation. However, the second model may have a substantially higher likelihood and thus posterior. The algorithm always accepts new sets if $p(N_{x+1}) \geq p(N_x)$. Critically, new sets with lower posteriors are sometimes accepted with probability $p(N_{x+1})/p(N_x)$.

The generation functions that we used to guess N_{x+1} are tuned to produce an overall acceptance rate of ~25% to 75%. We report results from Markov chains with 1.66×10^6 and 2.71×10^6 accepted links for the single- and two-stage models, respectively. Visual inspection of the output traces reveals that these chains have converged, meaning that each Markov chain is equivalent to a long series of random draws from the real posterior distributions. To remove any dependence on our initial guess of model parameters, we remove all links before the likelihood first dips below its eventual median. Only 434 and 445 links were deleted from the Markov chains for the single- and two-stage models, respectively. Extended Data Fig. 2 shows the distributions of chi-squared values for both models, along with the posterior distributions for Earth's bulk composition and constants governing partitioning behaviour. As desired, posteriors for these parameters are basically equal to the priors. The posterior for the bulk abundance of Ta peaks 1.58 standard deviations away from the estimated mean, but values within 1σ remain quite plausible. Extended Data Fig. 3 contains the posterior probability distributions for other parameters in the two-stage model.

Magnesium precipitation. We constructed a simple model for the precipitation of Mg-rich silicates and oxides. The output of this calculation is the mass of precipitate associated with a given amount of cooling, which is an essential parameter in the complete thermochemical model detailed below. At a given temperature, a condition for silicates and oxides to precipitate may be written as:

$$X_{FeO} + X_{MgO} + X_{SiO_2} \geq 1$$

where X_i are the mole fractions of three metal oxides that are calculated as functions of the mole fractions and exchange coefficients for Fe, Mg, and O in the core as follows[10–12,22]:

$$X_{FeO} = X_{Fe} \times X_O / K_O$$

$$X_{MgO} = X_{FeO} / X_{Fe} \times X_{Mg} / K_{Mg}$$

$$X_{SiO_2} = (X_{FeO} / X_{Fe})^2 \times X_{Si} / K_{Si}$$

Here we assume that precipitated material is instantaneously removed from the core. To generate Fig. 2, we begin with an undersaturated core at 6,000 K. We then decrease the temperature in increments of 1 K until precipitation begins. Next, we calculate how much of each oxide to remove to return the core to equilibrium. As temperature decreases further, the core gradually becomes depleted in light elements.

Thermochemical histories. Neglecting some small terms, the energy balance of the core is:

$$Q_{CMB} = Q_R + Q_S + Q_G + Q_{G'} + Q_L$$

where Q_{CMB} is the heat flux across the CMB, Q_R is the amount of radiogenic heating, Q_S is the magnitude of secular cooling, Q_G and $Q_{G'}$ are gravitational energy changes associated with inner-core growth and Mg precipitation, respectively, and Q_L is the latent heat released from phase transitions[26]. Heating due to dynamo activity is both generated and dissipated within the core and thus is not included. It is, however, important to the entropy balance[26]:

$$E_\phi + E_K = E_R + E_S + E_G + E_{G'} + E_L$$

Here E_ϕ, E_K and E_R are the entropy fluxes associated with ohmic dissipation, adiabatic heat flow, and radioactivity, respectively. The last four terms—E_S, E_G, $E_{G'}$ and E_L—are directly proportional to the rate of core cooling. We use parameterizations of these terms from Nimmo[26], plus our own estimates of the contribution from the precipitation of Mg-rich material detailed below. Other analytical models for the evolution of the core may imply higher initial CMB temperatures for dynamos driven by thermal convection alone[34]. Throughout, we assume that the thermal conductivity equals 130 $W\,m^{-1}\,K^{-1}$, based on the vast majority of recent studies[2–5], and that the abundance of potassium (K) in the core is 100 parts per million.

Combining the entropy and energy balances yields an expression for the heat flow across the CMB that is needed to drive a dynamo[26]:

$$Q_{CMB} = Q_R \left[1 - \frac{Q_T}{E_T}\left(\frac{E_R}{Q_R}\right)\right] + \frac{Q_T}{E_T}(E_\phi + E_K)$$

where the heat flow $Q_T = (Q_S + Q_G + Q_{G'} + Q_L)/(dT_{CMB}/dt)$ and the entropy $E_T = (E_S + E_G + E_{G'} + E_L)/(dT_{CMB}/dt)$ combine production terms that depend on the cooling rate. The temperature at the CMB is T_{CMB}. The implied cooling rate is $dT_{CMB}/dt = -(Q_{CMB} - Q_R)/Q_T$. If we assume a fixed value for E_ϕ, we can iterate these equations backwards in time from the present to calculate the thermochemical history of the core. Increasing the amount of entropy required for the dynamo or the adiabatic heat flow implies higher initial temperatures and heat flow.

© 2016 Macmillan Publishers Limited. All rights reserved

Radiogenic heating limits the amount of secular cooling, but actually mandates higher core-to-mantle heat flow to sustain a dynamo. In reality, the thermal evolution of the mantle determines Q_{CMB} and thus the amount of entropy available for the dynamo. By assuming that E_ϕ is fixed to a particular value, we are essentially computing the minimum heat flow that the mantle must be able to accommodate from the core.

The gravitational contribution to core heating from Mg precipitation may be estimated as:

$$Q_{G'} = \int_\infty \varphi \left(\frac{\partial \rho}{\partial t}\right)_{P,T} \mathrm{d}V = \int_\infty \varphi \rho \alpha_c \left[C_m \left(\frac{\mathrm{d}T_{CMB}}{\mathrm{d}t}\right)\right] \mathrm{d}V$$

where φ is the gravitational potential, ρ is density, t is time, and V is volume. The coefficient of compositional expansivity $\alpha_c = -1/\rho(\partial\rho/\partial c)_{P,T} \approx 1.12$, where c is the concentration of the light elements that precipitate out of the core. The rate of precipitation, C_m, is normalized to the initial core mass and directly proportional to the rate of cooling $\mathrm{d}T_{CMB}/\mathrm{d}t$. Since inspection of Fig. 2 suggests that about 0.5% of initial core mass precipitates per 100 K of cooling, we set $C_m = 5 \times 10^{-5}$. The exclusion of Mg from the inner core, if any, is already taken into account by using the empirical density difference across the inner-core boundary to calculate the gravitational contribution from the solidification of the inner core. The associated entropy flux[26] is simply $E_{G'} = Q_{G'}/T_{CMB}$. The entropy contribution from the latent heat of precipitation is exactly zero if precipitation occurs at the top of the core. Accordingly, we do not include any contribution from latent heat of precipitation in our calculation of Q_{CMB}. At present, $Q_L \approx 5$ TW and the rate of inner-core growth by mass is perhaps 2 to 4 times the amount of precipitation[26]. Including the latent heat of precipitation would possibly increase Q_{CMB} by 1–2 TW and slightly decrease the implied amount of secular cooling.

31. Nomura, R. *et al.* Partitioning of potassium into the Earth's core and implications for thermal history of the Earth. *AGU Fall Meet. Abstr.* DI33A–2411 (2012).
32. McDonough, W. F. in *Earthquake Thermodynamics and Phase Transformation in the Earth's Interior* (eds Teisseyre, R. & Majewski, E.) 3–23 (Academic Press, 2001).
33. Chib, S. & Greenberg, E. Understanding the Metropolis-Hastings algorithm. *J. Am. Stat. Assoc.* **49,** 327–335 (1995).
34. Labrosse, S. Thermal evolution of the core with a high thermal conductivity. *Phys. Earth Planet. Inter.* **247,** 36–55 (2015).

© 2016 Macmillan Publishers Limited. All rights reserved

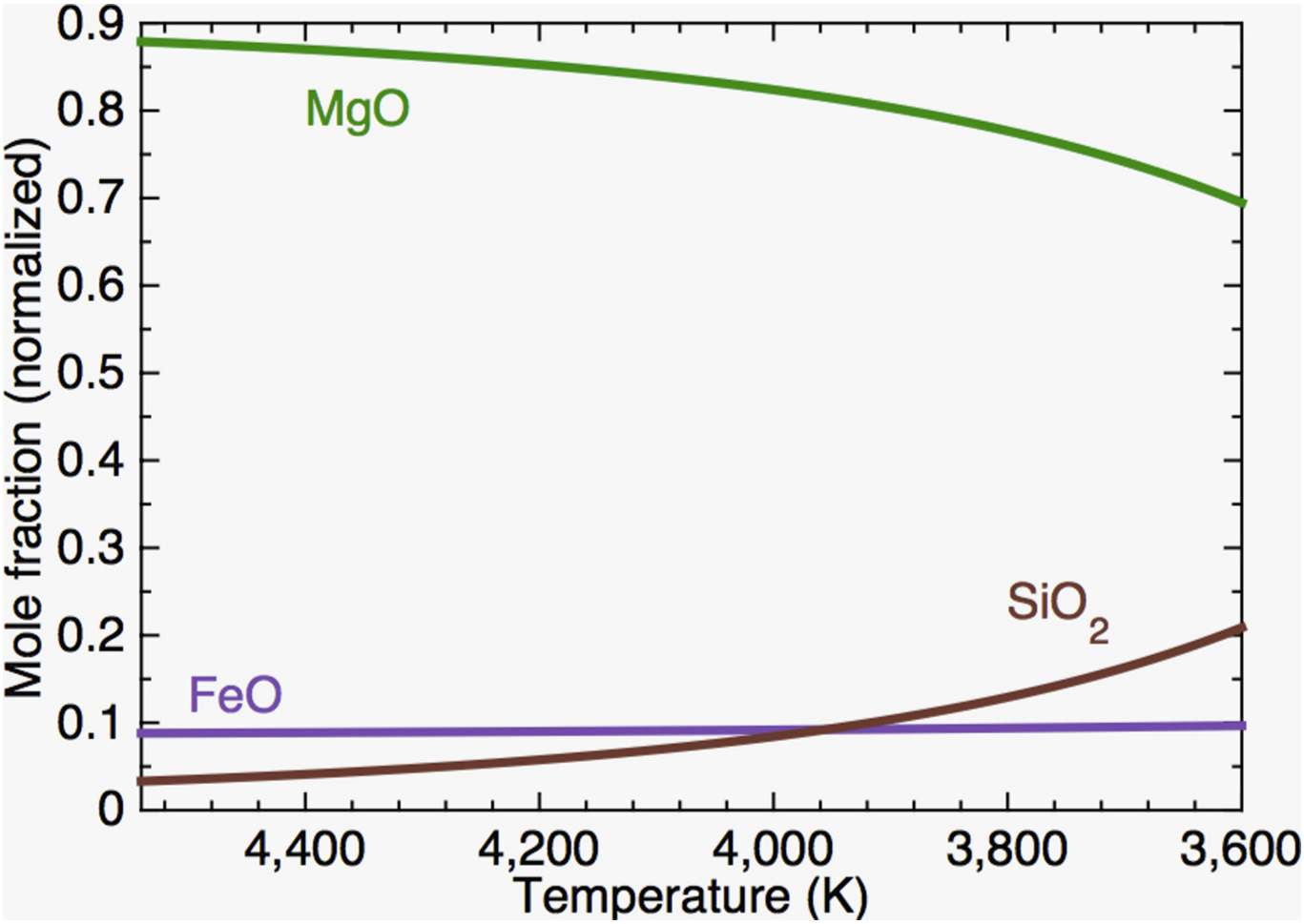

Extended Data Figure 1 | One example of the evolution of the composition of the precipitate. Here the core initially contains 2 wt% Mg, 3 wt% Si and 6 wt% O. Additionally, the constants a_O, b_O and c_O are each reduced by 0.25σ from their estimated mean values. The actual mineralogy of the precipitate (for example, the amount and composition of perovskite) is not modelled in detail.

© 2016 Macmillan Publishers Limited. All rights reserved

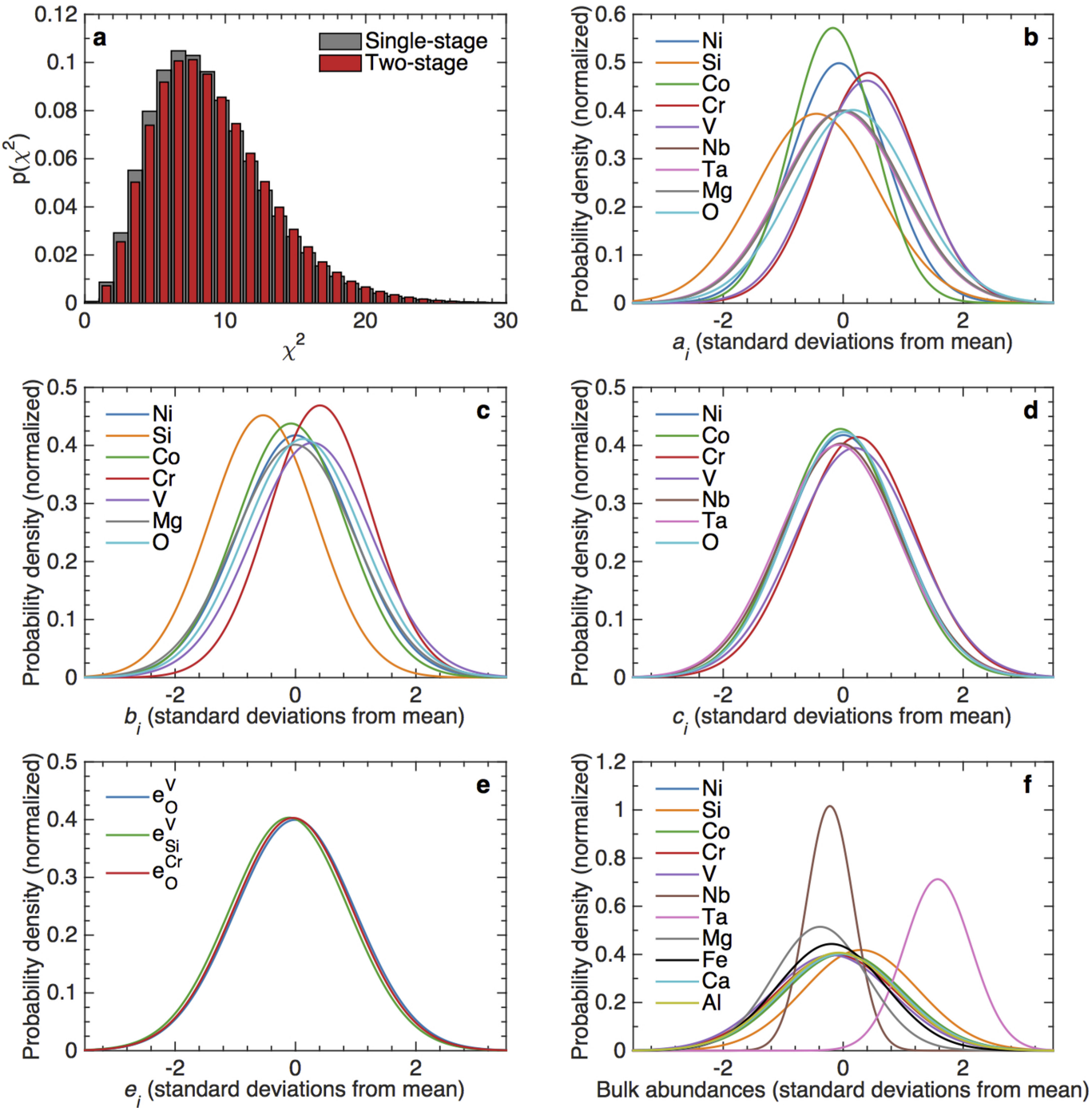

Extended Data Figure 2 | Additional results from models of Earth's core–mantle differentiation. Normalized distributions of chi-squared values, $p(\chi^2)$, for both models of core formation (**a**), along with posterior probability densities for the coefficients a_i, b_i, c_i, and e^i_j for various elements i and j used in the two-stage model to calculate partitioning behaviour (**b**–**e**) and elemental abundances in bulk Earth (**f**).

© 2016 Macmillan Publishers Limited. All rights reserved

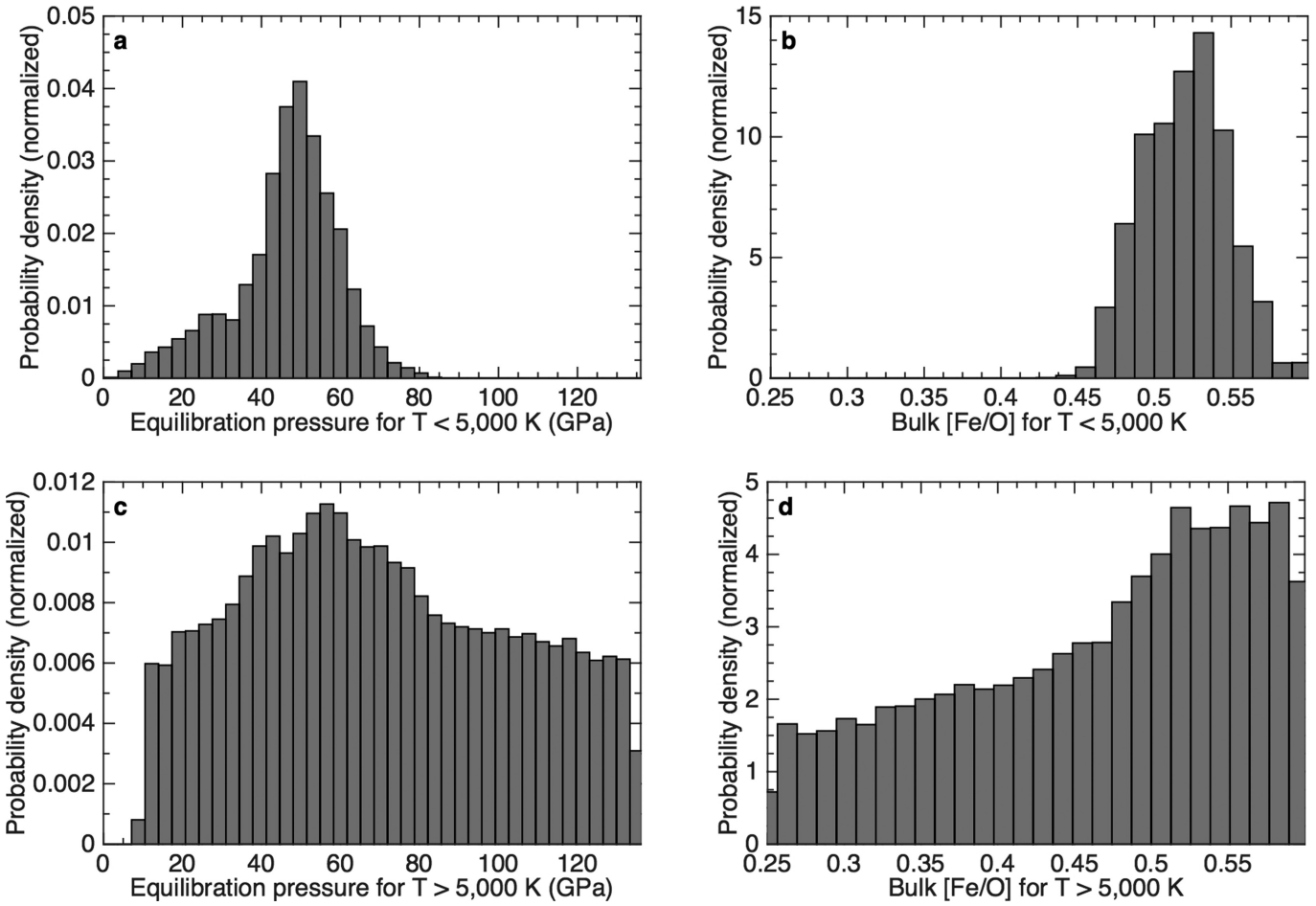

Extended Data Figure 3 | Posterior probability densities for parameters in the two-stage model of Earth's core–mantle differentiation.

© 2016 Macmillan Publishers Limited. All rights reserved

Extended Data Table 1 | Parameters with uncertainties used in models of Earth's differentiation

i	Bulk Earth	σ	Primitive mantle	σ	Units	n	a_i	σ	b_i	σ	c_i	σ
Fe	31.9	1.3	6.3	0.063	wt%							
Ca	1.71	0.10	2.61	0.21	wt%							
Al	1.59	0.10	2.38	0.19	wt%							
Mg	15.4	0.62	22.17	0.22	wt%	2	0.1	0.1	-10,851	1,000		
Si	16.1	0.48	21.22	0.21	wt%	4	1.3	0.3	-13,500	900		
Ni	1.82	0.13	0.186	0.009	wt%	2	0.46	0.16	2,700	300	-61	6
Co	880	35	102	5.1	ppm	2	0.36	0.15	1,500	300	-33	5
Nb	0.44	0.044	0.595	0.119	ppm	5	2.66	0.11	-14,032		-199	16
Ta	0.025	0.003	0.043	0.002	ppm	5	0.84	0.09	-13,806		-115	13
V	105	6.3	86	4.3	ppm	3	-1.5	0.3	-2,300	700	9	9
Cr	4,700	235	2,520	252	ppm	2	-0.3	0.2	-2,200	600	-5	7

The table shows the oxygen-free composition of bulk Earth[23], elemental abundances in the primitive mantle[32], and constants a_i, b_i, and c_i used to model partitioning behaviour[12,22]. For O, $a = 0.6 \pm 0.4$, $b = -3{,}800 \pm 900$, and $c = 22 \pm 14$. Likewise, $e_O^V = -0.077 \pm 0.008$, $e_{Si}^V = 0.039 \pm 0.014$, and $e_O^{Cr} = -0.037 \pm 0.007$, which are used to calculate temperature-dependent interaction parameters as described in ref. 22.

© 2016 Macmillan Publishers Limited. All rights reserved